PAPER

ELM frequency enhancement and discharge modification through lithium granule injection into EAST H-modes

IOP Publishing | International Atomic Energy Agency Nuclear Fusion

Nucl. Fusion **58** (2018) 126021 (13pp) https://doi.org/10.1088/1741-4326/aae2c1

ELM frequency enhancement and discharge modification through lithium granule injection into EAST H-modes

R. Lunsford[1,a], J.S. Hu[2,a], Z. Sun[1], R. Maingi[1], D.K. Mansfield[1], W. Xu[2], G.Z. Zuo[2], M. Huang[2], A. Diallo[1], T. Osborne[3], K. Tritz[4], J. Canik[5], X.C. Meng[6], Q. Zang[2], X.Z. Gong[2], B.N. Wan[2], J.G. Li[2] and The EAST team

[1] Princeton Plasma Physics Laboratory, Princeton, NJ 08543, United States of America
[2] Institute of Plasma Physics, Chinese Academy of Sciences, Hefei, Anhui 230031, People's Republic of China
[3] General Atomics, PO Box 85608, San Diego, CA 92186-5608, United States of America
[4] Johns Hopkins University, Baltimore, MD 21211, United States of America
[5] Oak Ridge National Laboratory, Oak Ridge, TN 37830, United States of America
[6] Department of Applied Physics, Hunan University, Changsha 410082, People's Republic of China

E-mail: rlunsfor@pppl.gov and hujs@ipp.ac.cn

Received 23 July 2018, revised 15 September 2018
Accepted for publication 20 September 2018
Published 10 October 2018

Abstract

The injection of impurity granules into fusion research discharges can serve as a catalyst for ELM events. For sufficiently low ELM frequencies, and granule sizes above a threshold, this can result in full control of the ELM cycle, referred to as ELM pacing. For this research, we extend the investigation to conditions where the natural ELM frequency is too high for ELM pacing to be realized. Utilizing multiple sizes of lithium granules and classifying their effects by granule size, we demonstrate that ELM mitigation through frequency multiplication can be used at ELM triggering rates that nominally make ELM pacing unrealizable. We find that above a size threshold, injected granules promptly trigger ELMs and commensurately enhance the ELM frequency. Below this threshold size, injection of an individual granule does not always lead to the prompt triggering of an ELM; however, collective ablation in the edge pedestal region does enhance the ELM frequency. Specifically, Li granules too small to individually trigger ELMs were injected into EAST H-mode discharges at frequencies up to 2.3 kHz; collectively the granules were observed to enhance the natural ELM frequency up to 620 Hz, resulting in a ~2.4 × multiplication of the natural ELM frequency and a 50% decrease of the ELM size.

Keywords: ELM, pacing, lithium

(Some figures may appear in colour only in the online journal)

1. Introduction

The advancement of the world fusion program towards ITER and other similar class devices leads to a situation whereby the energy contained within the core plasma and exhausted during steady state operation challenges the engineering capabilities of boundary plasma facing components (PFCs) [1, 2]. As such, excursions above the steady state heat load are more problematic than in present devices. In the standard high confinement mode (H-mode), planned as the ITER baseline operational scenario, the periodic plasma relaxations known as edge localized modes (ELMs) create localized high temperature strike points that can exceed material structural tolerances [3]. The energy stored within large 'Type 1' ELMs (ΔW_{ELM}) accompanying high performance H-mode operation can often be 10%–15% of the total stored energy (W_{TOT}) [4]. These bursts lead

[a] The first two authors should be considered as equal co-authors.

to enhanced thermal stresses, component fatigue and material sputtering from the PFCs, which can cause unacceptably short component lifetimes. Research has shown [5] that the primary material damage resulting from ELMs is caused by the peak heat flux. To ameliorate these effects we take advantage of an observed inverse relationship between the frequency of the ELMs and their peak heat flux. Thus if ELM frequencies can be stimulated to sufficient levels, the peak heat flux should be mitigated to acceptable values.

Present ITER plans call for ELM pacing using high frequency deuterium pellet injection as one of the baseline ELM mitigation strategies [6]. However, frequency enhancement using fuel pellets poses additional fuel processing requirements for DT discharges due to strict regulation of system tritium levels. Thus limits operational scenarios to discharges which satisfy the two competing limitations of fuel throughput and ELM frequency multiplication. However, if an alternate method can be utilized to augment the pacing effect achieved by pellet injection, a decoupling of ELM pacing and fueling might be achieved, thus potentially expanding the operational parameter space.

In addition to the other ELM mitigation methodologies planned for ITER [7], the injection of impurity granules has been studied as a means to both provide density control through augmenting the natural ELM frequency as well as mitigating the effects of ELMs on the PFCs. To augment the natural ELM frequency of EAST H-mode discharges, we injected spherical granules with diameters ranging from 1 mm to 200 microns at frequencies from 70 Hz to over 2300 Hz. For those instances where the granule diameter was larger than 600 microns, prompt triggering of individual ELMs was observed. These injections boosted the ELM frequency by 36%, from 275 Hz to 375 Hz. Granules with diameters ranging from 400–600 microns were determined to be close to the ELM triggering threshold, with triggering efficiency ranging from 40%–95%. However, due to a faster granule injection rate ($\leqslant$1.2 kHz with these smaller sizes), the ELM frequency was increased from baseline levels ~250 Hz to ~600 Hz. In addition the peak $D\alpha$ amplitude, used as a proxy for ELM size, was reduced by 44%. When the injected granule diameters were further reduced below the threshold band, a direct correlation between the injection of a particular granule and the triggering of a specific ELM could not be established. However, when viewed collectively there was a substantial augmentation to the baseline ELM frequency. Because of the design of the dropper section of the granule injector, the smallest granules were able to be injected at substantially greater frequency than their larger counterparts. As such an injection frequency of approximately 2300 Hz boosted the ELM frequency to over 600 Hz, more than doubling the natural ELM frequency. This resulted in a reduction in the peak $D\alpha$ signal by more than 50%.

In the remainder of the paper we first describe the EAST tokamak and the granule injector apparatus. We then present the global effects of granule injection onto the discharges and examine the variations in plasma response resultant from a variation in granule size. We conclude by describing how these effects, along with the enhanced frequency rate seen with smaller granules, results in a mitigation of the ELM size as shown by the measured reduction in peak $D\alpha$.

2. EAST Tokamak and baseline discharge parameters

One of the primary missions of the experimental advanced superconducting tokamak (EAST) [8] is to demonstrate stable 1000 s-long H-mode discharges and thus provide critical physics and technology verification for ITER and the china fusion engineering test reactor (CFETR) [9]. To accomplish this mission EAST is equipped with dominant RF heating (lower hybrid wave (LHW) and ion cyclotron resonant heating (ICRH)) and a tungsten monoblock upper divertor capable of exhausting 10 MW m^{-2} to enable long-pulse experiments [10]. To manage the energy exhaust from these discharges, specifically peak heat fluxes resultant from ELMs, EAST is equipped with a full complement of ELM control mechanisms. These include: lithium wall conditioning [11], lithium aerosol injection [12], supersonic molecular beam injection (SMBI) [13], resonant magnetic perturbations (RMP) [14], deuterium pellet injection [15], as well as the lithium granule injection system utilized in these experiments.

The nominal major and minor radii of EAST are 1.9 m and 0.45 m respectively. The experiments described in this paper were undertaken with an average stored energy of 175 kJ and plasma current of 400 kA as shown in figure 1. These conditions are maintained by 6.2 MW of auxiliary heating as shown in panel (*b*). Primary energy deposition was provided by lower hybrid heating ($P_{\mathrm{LH1@4.6\,GHz}} = 2$ MW, $P_{\mathrm{LH2@2.45\,GHz}} = 0.3$ MW) and neutral beam injection ($P_{\mathrm{NBI}} =$ ~3.5 MW), with additional heating from the electron cyclotron resonant heating system ($P_{\mathrm{ECRH}} =$ ~0.3 MW). Average plasma densities of 2.5×10^{19} m^{-3} were feedback-controlled via SMBI, which has been observed [13] to augment ELM triggering frequencies. Control of recycling and edge impurity influx was provided by daily evaporative lithium coatings. For discharges without granule injection, the natural ELM frequency was approximately 250 Hz. It has been observed [16] that the average energy loss from uncontrolled type I ELMs on EAST is approximately 8%.

3. Granule injector system and ELM triggering

3.1. Injector description

The lithium granule injector (LGI) [17], developed by PPPL [18] and first installed on EAST [19], is a combination of a piezoelectric granule dropper [20] with a rotating turbine impeller. The granules are stored in a 4-chamber reservoir containing the 300, 500, 700, and 900 micron ($\pm$100 microns) diameter sizes. The active chamber is mechanically selected and the granules are fed onto a piezoelectric disk, which, when vibrated at resonance, drives the granules to a central aperture and into a waiting drop tube. Upon entering the drop tube the granules are gravitationally accelerated and enter the injection chamber directly above a dual-bladed rotating turbine

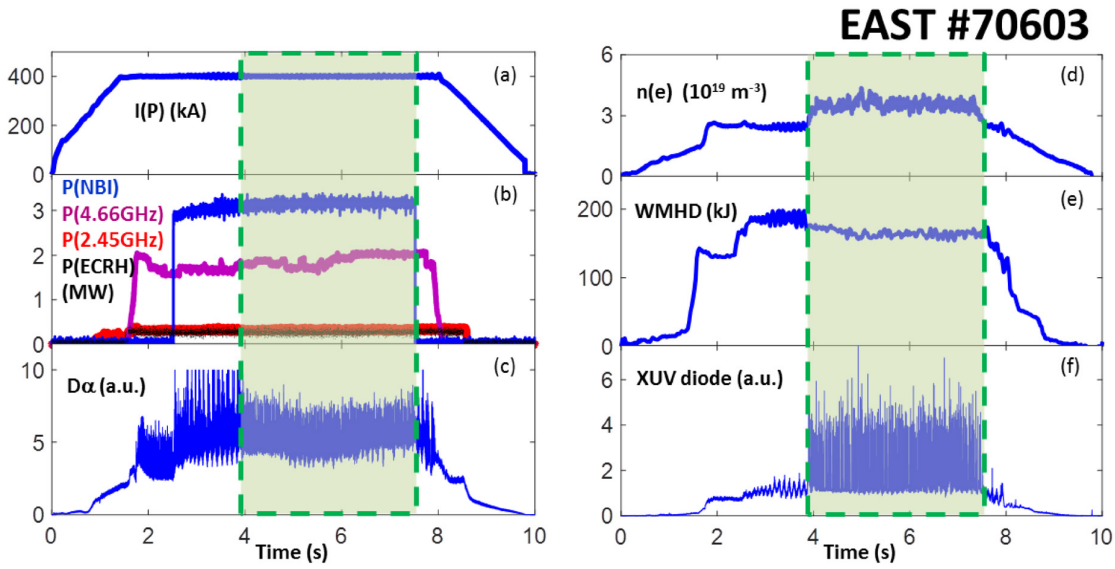

Figure 1. Typical discharge parameters for EAST granule injection experiments. Granules are injected from 4–7.5 s, as highlighted by the colored boxes overlaid on the diagnostic traces.

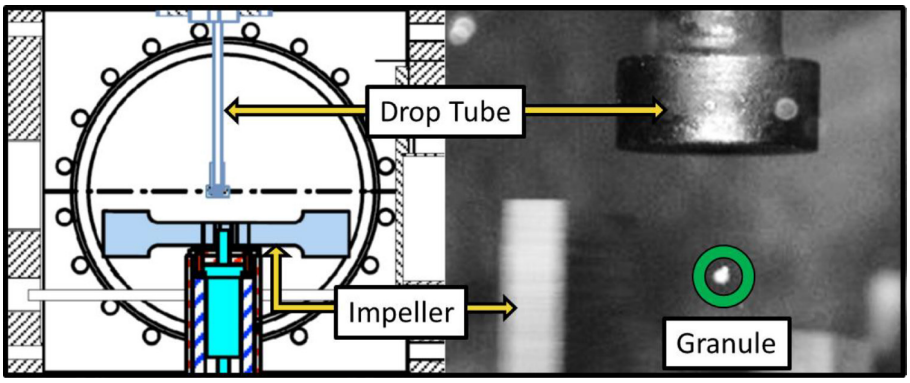

Figure 2. Granule injection schematic and image. The left hand frame displays a drawing of the injection chamber. Granules exit the drop tube and are horizontally driven into the discharge by a dual-blade impeller rotating from left to right. The image at right displays a representative still frame from a dedicated framing camera. The square outlines a section of the dropper head which provides a reflection of the discharge and is used to monitor granule ablations.

impeller, which drives the granules horizontally into the low field side of the discharge. The roughly 370 Hz impeller rotation frequency corresponds to an injection velocity for the granules of approximately 80 m s^{-1}, with variability of ± 5 m s^{-1} owing to fluctuations in impeller frequency and injection angle.

For these experiments, the piezoelectric disk which is used to drive granules to the drop tube was maintained at a constant voltage. This single voltage provides a more efficient coupling to the smaller granules as compared to the larger ones, and as such smaller granules enter the drop tube at a much higher rate than their larger counterparts.

3.2. Diagnostic suite

To determine the effect of the granules upon the EAST discharge, it is necessary to quantify the number, frequency, size and velocity of the injected granules. To do so, the granule injector is equipped with a diagnostic suite and customized analysis package which tracks both the collective behaviour of the granule train as well as single granules from the point of introduction at the base of the drop tube through completed ablation within the discharge. Granule injection parameters are determined through analysis of the externally illuminated injection chamber images as provided by a high speed framing camera. A sample image is shown on the right hand side of figure 2. These images record the number and size of granules falling from the drop tube, as well as monitor the rotation frequency of the impeller blade from which the injection speed of the impacted granule is calculated. Granule ablation characteristics are observed by a second dedicated camera with a wide angle view, along with other EAST diagnostics.

3.2.1. In situ granule size measurements. Granule size is the most significant control variable in determining individual effects upon the discharge. When injected at roughly

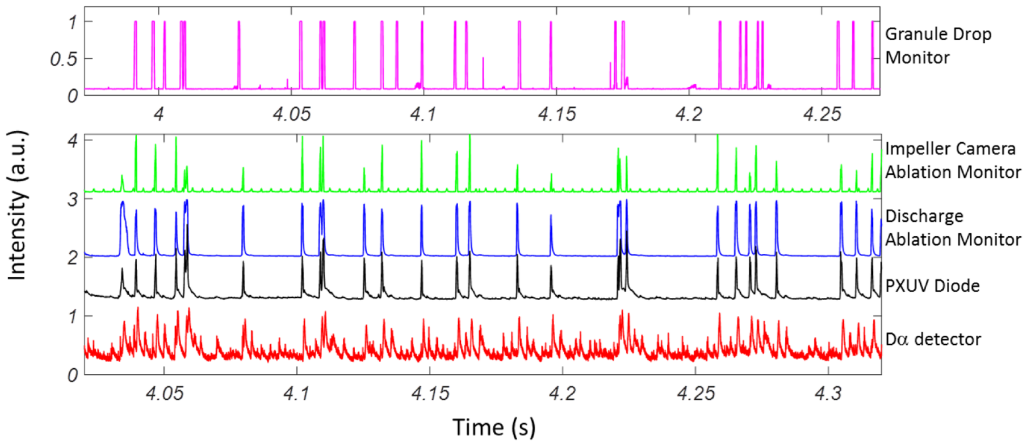

Figure 3. Granule tracking from injection through ablation and ELM triggering for discharge EAST 70603. Moving from top to bottom the granule is tracked from its exit from the drop tube, its ablation is recorded on both the impeller and ablation cameras, which is then correlated to the PXUV diode signal, confirming the injection. If the granule is successful in triggering an ELM, the resulting spike will appear in the Dα trace as shown by peaks on the lowermost trace. The delay in the time base between the first trace and remaining 4 signals reflects the time required for the granule to transit the flight tube and impact the edge plasma.

equivalent velocities, larger granules penetrate deeper than smaller ones, introducing a larger mass fraction into the discharge. Thus, to better correlate discharge effects to injection events, it is critical that granule size be estimated too better accuracy than the 200 micron 'bins' into which the granules had been sorted. This provides a particular challenge since the granules must be measured *in vacuo* immediately prior to injection to quantify this mass deposition effect. As the resolution of the injection chamber image is 135 microns per pixel, on the order of the smallest granule size, we employ a sub-pixel analysis technique to estimate granule diameter. Given that the camera and illumination source are far from the granule we approximate the illumination response of the light scattered from the granule (I_g) to be proportional to the circular surface area of the granule $I_g \sim \pi r_g^2$. Here α is the geometric collection factor of the optics, a first order constant over the granule radii (r_g). The largest granules were utilized for calibration because they illuminate the largest number of image pixels. During EAST discharge #70601, 169 individual granules were dropped into the injection chamber. Assuming a uniform size distribution for the group and average diameter of 900 microns, we utilize the average dropped granule response to calculate an optical collection factor $\alpha = 0.044$. This factor was then used to determine the sizes of the remaining granules to within an accuracy of half a pixel (~70 microns). We also note that while the lithium granules have been observed to deform during impact with the impeller, they do not fracture. Thus each granule that is dropped retains its integrity and is maintained as a single granule throughout injection.

3.2.2. Granule tracking and ablation monitoring. The calculated granule velocity is based on both the rotation speed of the impeller and a coefficient of restitution, C_R: a measure of the inelasticity of the paddle-granule collision [21] for lithium granules of 0.3 using the equation $v_g = (1 + C_R) * (2\pi r_i * f_i/2)$, where r_i and f_i are the radius and frequency of the impeller respectively. This calculation has been verified by examining the displacement of granules between frames as they transit the injection chamber.

The ablation of the granules was monitored in several ways. From previous LGI experiments [17] we have determined that there is a section of metal on the end of the drop tube that reflects an image of the horizontal injection tube which the granules traverse on their way to the discharge (see figure 2 with the red square). The reflection creates a low resolution image of the EAST plasma which, due to the luminosity of the ablating granules, confirms successful injection. If the granule frequency is sufficiently low, this method can be used to confirm time of flight and as an independent check on the calculated granule velocity values inferred from inelastic collision with the rotating impeller [22]. The second method of ablation monitoring is through a dedicated Vision Research Phantom V710 high-speed camera which directly observes the discharge through a window adjacent to the granule injector. The camera images the extent of the ablation cloud surrounding the granule and provides a record of the ablation duration. Finally, once the granule enters the discharge, it generates a sharp peak on the XUV diode diagnostic, and if the granule is successful in triggering an ELM, a corresponding peak can also be seen on the $D\alpha$ filterscope trace.

By following figure 3 from the uppermost trace, down through subsequent traces, the granule history can be ascertained. The top trace is a summation of a linear array of pixels located directly below the end of the drop tube as recorded on the impeller camera. Peaks recorded on this trace provide a read-out of the granules prior to impact with the impeller. The second trace is also a summed pixel array subset of the impeller camera image; however, this subset of the image is dedicated to a region on the dropper head utilized to monitor ablations, as described above and in [16, 22]. The offset in the time base between the first and second trace corresponds to the transit time of the granule down the flight tube of the LGI prior to connecting with the edge of the discharge. Note that there are spikes which occur on the upper 'Granule Drop

Table 1. Granule injection parameters and resultant effects on ELM frequency. The table displays the size as calculated from impeller camera measurements, duration of ablation as recorded by a plasma viewing camera to a resolution of ± 50 μs, the frequency of ablation events as recorded by the XUV diode array, and a comparison of the $D\alpha$ resolved ELM frequency both prior to and during granule ablation events. A comparison of the XUV and $D\alpha$ traces results in the prompt ELM triggering efficiency. The elevation of ELM frequency due to granule injection is the granule pacing factor as described in section 3.4.

Shot number	Average granule size (microns)	Granule drop frequency	Granule injection frequency (Hz-XUV)	Average duration of ablation (ms)	Pre-granule ELM frequency (Hz)	Granule assisted ELM frequency (Hz)	Prompt ELM triggering efficiency (%)	Granule pacing factor (%)
70601	900	89	83	1.42[a]	285	376	100	110
70602	900	85	77	0.91	301	372	100	92
70603	810	135	110	0.95	263	315	99	47
70604	800	153	130	N/A[b]	250	314	99	49
70605	610[c]	593	430	0.69	232	442	86	42
70606	460	1239	780	0.51	283	623	64	32
70607	260	2372	920	0.4	257	631	21	19

[a] Ablation camera exposure per frame was 4.5 × longer for this set of injections leading to a longer saturated phase where the status of the granule was occulted by a radiative lithium cloud.
[b] Ablation camera results not recorded during this discharge.
[c] Granule size was varied over the course of the injection, values in this row represent an average over full injection duration. See section 4.3 for further discussion.

Monitor' trace which have no corresponding ablation events. These are indications of granules which are driven at oblique angles to the injection tube, and do not enter the boundary plasma. Overall, the injection efficiency, defined as the ratio of ablated granules to granules dropped, was found to be approximately 85%. This quantity was determined for the largest granules, where only a single granule was injected per impeller pass, and assumed to apply for the smaller granules, where higher granule throughput allowed the possibility of multiple granules contacted per impeller pass. This assumption allows an estimation of the number of small granules injected during periods when it was more difficult to ascertain the success of an individual injection due to the presence of multiple granules per impeller pass.

The third trace is an integrated intensity of the dedicated discharge monitor camera and these observed ablation events directly correlate with the XUV diagnostic trace shown in the fourth signal. The XUV trace is utilized to confirm granule injection in the event that the ablation of the granule occurs outside the field of view of the ablation camera. If the granule is successful in triggering an ELM, then a corresponding peak can be seen on the $D\alpha$ filterscope trace, which is displayed as the bottom signal on the figure.

3.3. Granule injection parameters

The observable granule parameters during a size and frequency injection scan is compiled in table 1. Given the duration of ablation for the granules and an average injection velocity of 80 m s^{-1}, we can estimate the farthest extent of granule penetration. For the largest granules injected into EAST this corresponds to a depth of 7.8 cm from the edge of the discharge, a point just past the steep gradient region in the H-mode pedestal. The 3rd and 4th columns record the average frequency of the granules as they exit the dropper and the injection frequency as they enter the discharge as measured by peaks on the XUV diagnostic signal. For the larger granules, which are primarily driven into the discharge as single granules, this provides a measure of the efficiency of the granule injector in delivering material into the discharge. As reflected in the table, there is an inverse relationship between granule size and injection frequency, due to the design of the injector. As a consequence, the smaller granules, which are driven more efficiently by the disk vibrations, enter the drop tube at a greater rate. This effect was anticipated and a calibration of the inverse relationship between the granule size and the drop frequency was previously reported [18]. When the granule drop frequency exceeds the impeller rotation frequency of 370 Hz, multiple granules can be injected per impeller pass. The effects of these multiple injections depend on the regularity of their occurrence and are further described in section 4.4. When only a few granules are injected per impeller pass, variations in their injection trajectories result in distinct arrival times that allows the accounting of individual granules. However, this is not possible for the smallest granules where the number injected per impeller pass can range from a single granule up to 34 simultaneous granules.

3.4. Granule pacing factor

Previous experiments with the impurity granule injection focused on the ability to fully control the ELM cycle through the concept of ELM pacing [23]. In these cases each individual granule injection was termed successful or unsuccessful based upon its ability to promptly trigger an ELM. In addition it was also necessary that any spontaneous inter-granule ELMs be suppressed due to the elevated triggering rate. As such the only ELMs occurring could be identified as a direct result of granule injection. This could be accomplished under scenarios where the natural ELM frequency was low, on the order of tens of Hz, such that the elevated rate of injection for the largest granules, on the order of 100 Hz would completely dominate the ELM cycle. However when the natural ELM frequency is on the order of 200–300 Hz, such complete control could not

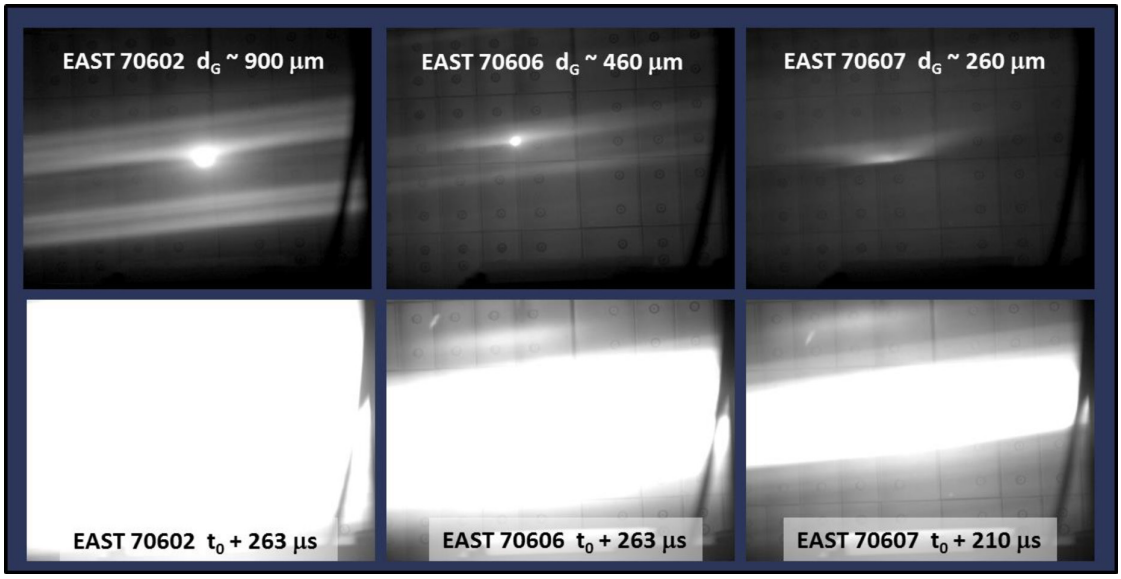

Figure 4. Images of a granule ablation events as recorded by a dedicated high speed framing camera for three distinct granule sizes from three separate discharges. Each top row image (at t_0) of the ablating granule and resultant neutral cloud is recorded during the frame immediately before the ionized material becomes field aligned and optically saturates some or all of the frame. Saturated images and extent of the ablation cloud are shown in the images along the bottom row.

be realized with the present injector. Therefore we employed a new tactic—different from ELM pacing—and focused instead on an *augmentation* of the natural ELM frequency through small (in some cases sub-threshold) granule injection. The 6th and 7th columns of table 1 reflect this increase in ELM frequency as a result of granule injection.

Here we introduce the granule pacing factor ($\varkappa$) which characterizes the effectiveness of a series of granules in boosting the ELM frequency. This factor is defined as the difference between the ELM rate observed during injection $f_{\mathrm{ELM}}\,(\mathrm{gran})$ and the pre-granule ELM rate $f_{\mathrm{ELM}}\,(\mathrm{pre})$ divided by the frequency of granule injection f_{GRAN}.

$$\varkappa = \frac{f_{\mathrm{ELM}}\,(\mathrm{gran}) - f_{\mathrm{ELM}}(\mathrm{pre})}{f_{\mathrm{GRAN}}}.$$

The final column of table 1 reflects the change in $\varkappa$ as the granule size is reduced. This method better represents the overall effect of the granules on the discharge. For granules above 800 microns, the granule injection rate (as quantified by peaks on the XUV data) was used as the metric for positive confirmation of full granule injection. However this method is unable to distinguish simultaneous granule injections. Thus for the smaller granules, which undergo multiple injections per impeller pass, the accounting of f_{GRAN} likely undercounts the number of individual granules injected. To compensate for this problem in EAST discharges 70605–70607, granules were individually counted as they impacted the impeller and then the granule drop frequency was multiplied by the nominal injection efficiency of 85%, thus generating an estimate of the number of granules injected. It is this number that was then used for the granule injection frequency in the pacing factor calculation.

3.5. Granule ablation and ELM triggering

The mechanically injected granules rapidly transit the scrape-off layer and enter the pedestal region. Once in the pedestal, the granule encounters a field-constrained fast-electron fluence which rapidly sublimates the surface layer. Many experiments have shown [24–26] that these impurity granules then follow a neutral gas shielding model [27–29] of ablation similar to cryogenic deuterium pellets, albeit with a smaller neutral gas shielding factor. In this model the ablated neutrals form a shielding cloud around the granule and thus moderate the incoming heat flux to the surface. As the heat is absorbed by the neutral cloud, ionization occurs and the ions become tied to magnetic field lines and free stream away from the granule at the sound speed. The ablation of multiple-sized granules can be observed in figure 4. The top row of images shows a series of granules with a surrounding neutral cloud. The images presented are taken directly before the granule begins generating the field aligned ionized flux tube which indicates a crossing of the separatrix. The lower row of images shows the corresponding extent of the ablatant cloud as the granule transits the pedestal. The images are provided by a high speed camera, filtered to observe the 548 nm Lithium line, and aligned to observe radially inward roughly along the flight path of the granule. As the granule transits deeper into the edge plasma, the deposited material rapidly reaches a thermal equilibrium, and as density efflux is limited by cross field transport, this creates a pressure perturbation which can lead to an overdense flux tube. If sufficient material is deposited, this flux tube can then be driven to become locally ballooning unstable, which can trigger an ELM. The entrained plasma mass then transports the majority of this energy to the divertor [30]. The generation

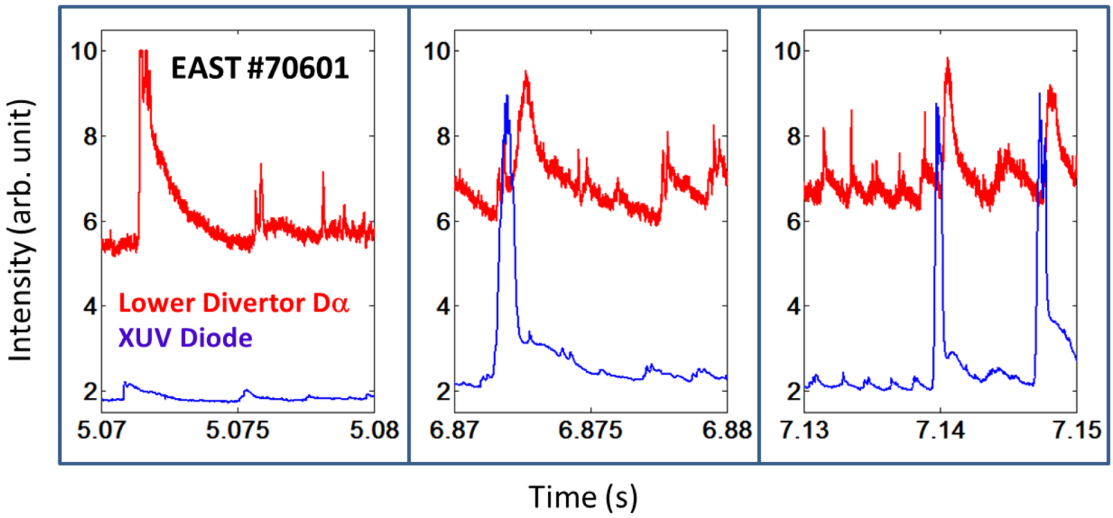

Figure 5. Comparison of spontaneous and simulated ELMs. The left panel shows a spontaneous ELM (i.e. not involving granule injection). Note that the $D\alpha$ detector saturates at a 10 V signal level, obviating a full determination of peak intensity. The middle panel shows the XUV diode signature of a granule ablation and the resultant promptly triggered ELM. The right panel displays a combination of mitigated spontaneous ELMs interspersed with granule-induced ELMs.

of ELMs by this pressure perturbation method was highlighted by simulations of pellet injection with the JOREK code [31].

Previous experiments with the injection of granules have not noted any substantive difference between natural and granule-stimulated ELMs [19, 22]. As is shown in figure 5, the overall envelope and magnitude of the two events in $D\alpha$ light are similar. The left panel shows a natural ELM, without the corresponding signature of a granule on the XUV diode. The middle panel shows a later time in the same discharge where the ELM is triggered by a granule injection. The right panel is representative of a train of rapid natural ELMs interspersed with a pair of granule triggered ELMs. In addition, research at DIII-D [32] has demonstrated that there is little correlation between injected granule size and the resulting triggered ELM size. The combination of the DIII-D observations with the similarity of the spontaneous and stimulated ELMs leads us to the conclusion that, for these experiments, ELM triggering is a two-step process. Nominally, that once the triggering threshold has been reached either by a granule or through the natural evolution of the pedestal, then the energy contained within the resultant ELM is a dependent on plasma conditions and relatively independent of the triggering mechanism.

Thus, for the following analysis we do not differentiate between triggered and spontaneous ELMs. This approach also ameliorates the concern about causality which occurs when discussing the 'pacing' of ELMs, i.e. that each injected granule led to the triggering of an ELM, thus establishing full control over the ELM cycle. In such a discussion the concern exists that a particular ELM was temporally but not causally related to the injection of a granule, and due to the similarity of the signals between spontaneous and stimulated ELMs can be difficult to address. This type of control can be seen in experiments performed on DIII-D with Lithium granule injection [23, 32]. However, in this work—addressing the concept of ELM frequency augmentation—there is no such concern, primarily due to the elevated rate of spontaneous natural ELMs. Thus we focus on the differences that occur within the global ELM frequency during periods of granule injection. As such when discussing the ELM triggering frequency we are referring to the frequency corresponding to all ELMs, not just those that are individually induced by a granule and it is that frequency which we utilize when comparing the peak $D\alpha$ levels when measuring any sort of heat flux mitigation.

3.6. ELM peak heat flux mitigation through elevated ELM triggering rates

Previous research has shown [33] an inverse relationship between ELM frequency and the peak heat flux contained within the mode in certain operating scenarios. While the efficacy of ELM mitigation through frequency multiplication appears to be reduced in full metal machines [34, 35], it remains a baseline ELM mitigation technique for ITER. We thus examine the effects of granule-induced frequency enhancement of the ELM cycle with an eye towards mitigation. Divertor heat loads are nominally measured by utilizing a fast infrared (IR) camera viewing the lower divertor. However as the natural ELM frequency for these discharges is greater than 230 Hz, the resulting energy contained within a single ELM is only $\sim\Delta W/W_{\rm tot} < 1\%$–$2\%$, and as such cannot be individually resolved either by equilibrium reconstructions or by IR thermography. An alternate method of performing a relative comparison of ELM peak intensity is to examine the amplitude of the divertor $D\alpha$ signal. For example, during EAST 70606, granule injection boosts the ELM frequency from 300 Hz to 600 Hz, as is shown in the upper two panels of figure 6. This increase in ELM frequency leads to a reduction in the signal over baseline as recorded by the $D\alpha$ photodiode from ~4 V to approximately 2.75 V. This reduction of 1.5 $\times$ is roughly comparable to the 2 $\times$ increase in ELM frequency.

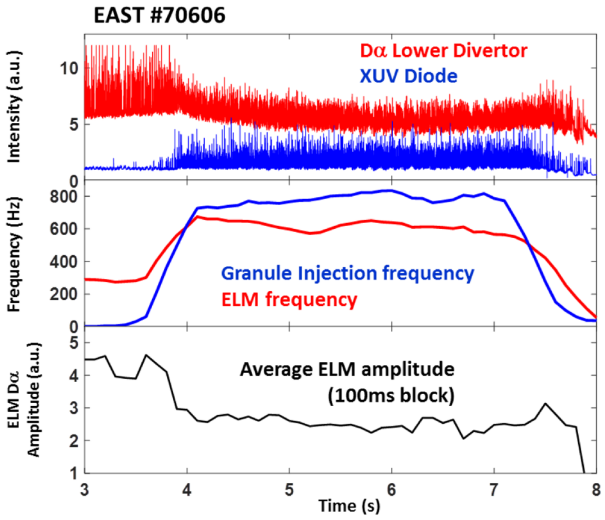

Figure 6. ELM mitigation through granule pacing effects. The injection of granules from 4 to 7.5 s has a distinct impact on the amplitude of the $D\alpha$ signal. The 780 Hz granule injection frequency, as recorded by the XUV diode, increases the ELM frequency from just under 300 Hz to just over 600 Hz and the amplitude of the ELMs over the baseline $D\alpha$ level is reduced by a factor of 1.5 $\times$ from 4.25 to 2.75.

This boost in ELM frequency comes at a κ of 32% which means that on average there is one ELM triggered for every 3 granules injected. The $D\alpha$ filterscope channel used for these measurements was chosen for sensitivity of response, thus allowing a better characterization of the behavior during the granule injection period. As a result of the high detector sensitivity, during pre-granule injection periods the signal can be seen to periodically saturate at 10 V, thus the mitigation numbers quoted here likely underestimate the ELM size reduction.

4. Effects of lithium granule injection on discharge performance

To examine the effects of lithium granule injection on discharge performance we subdivide the analysis into distinct sections. The first section describes effects on the discharge common to all granule injection shots, such as increases in density, ELM frequency, and lithium concentrations. Subsequent sections consist of an exploration of the effects due to different size granules. Instances where the injected granule has a 95% + chance of promptly triggering of an ELM are termed 'super-threshold' as they can be seen to reliably result in ELM events irrespective of discharge conditions. This is followed by an analysis of threshold granule injection. Injections within this band have a range of granule triggering probabilities from 40%–95%. Included in this analysis is an experiment where the average injected granule size was varied over the course of the discharge to provide a range of granule triggering efficiencies. The third type of injection experiments were done with 'sub-threshold' granule injection. In these instances the individual granules themselves were unable to be causally linked to the triggering of a specific ELM however there is a substantial increase in the overall discharge ELM frequency.

4.1. Overall effects of granule injection

The introduction of a localized impurity source via granule injection has an effect upon both the local and global plasma behavior. Figure 7 displays several key parameters during EAST 70606 and compared to the baseline discharge EAST 70600. The injection of granules results in a marked density rise as seen in the second panel. Stored energy (W_{MHD}) and β_p are both slightly elevated during the granule injection discharges, however as this occurs during the course of the entire discharge and is not constrained to the granule injection period, it is most likely due to cumulative lithium deposition and wall conditioning from the previous discharges and its positive impact on plasma performance [36–38]. Furthermore, despite the expenditure of energy required to ablate and ionize the impinging granules, which for 400 micron granules injected at 1053 Hz (1291 Hz $*$ 85% injection efficiency) is estimated at 66 kW, W_{MHD} only drops by approximately 15% and β_p is only reduced by 8%. This assumes that all the deposited granule mass remains entrained within this discharge; however studies have shown that a majority of the granule mass can be promptly exhausted from the boundary during the evolution of an ELM [39].

Examining the upper right two panels it becomes apparent the effect the rapid granule injection has on the ELM signature. As discussed above, the ELM amplitude decreased by nearly a factor of 1.5 as a result of rapid granule injection. This is compared to the discharge without granule injection which shows a constant ELM amplitude and unilateral baseline rise. As expected, the injection of lithium granules into EAST H-mode discharges substantially increased the lithium within the discharge. However due to the low atomic number and relatively small ionization energies of Lithium, the radiated power of the discharge only increased by 20%.

One of the primary effects of an injected granule is the possibility of the prompt triggering of an ELM [22]. As shown in figure 8, the injection of a granule of diameter larger than 600 microns will nominally result in the prompt triggering of an ELM. However the triggering efficiency substantially decreases when the granule diameter is reduced below 600 microns. Since the effect of a granule injection *vis-a-vis* the triggering of an ELM is a binary event, determination of a fractional triggering probability can only be performed in an ensemble sense. Thus the data points shown in figure 8 represent the average size and triggering efficiencies for a 100 ms discharge subset. As is shown, the triggering efficiency varied between 40% and 95% for the range of granule sizes between 400 and 600 microns. A portion of this effect can be attributed to the interpolation of large and small granules during discharge EAST 70605, as will be discussed in section 4.3. Additionally, as these granules are closer to a threshold value, the timing of the granule injection with respect to the position of the discharge during its natural ELM cycle evolution should also play a role in the effectiveness of a particular granule in ELM triggering.

Below a diameter of 400 microns, the probability of an individual granule triggering an ELM is decreased to 20% on average. In addition, due to the increased rate of granule injection, the probability that an ELM may be triggered

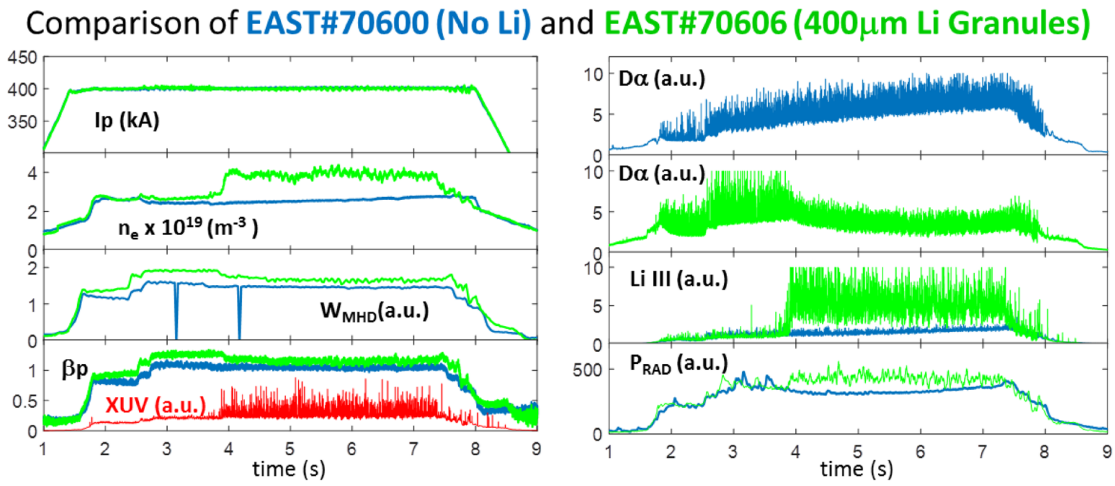

Figure 7. Comparison of discharge parameters in response to Li granule Injection. The plots on the left hand side and the bottom two plots on the right hand side display a comparison of particular characteristics for EAST discharge 70600 (blue) which was performed without granules and EAST discharge 70606 (green) which contained granule injection. The top two panels on the right hand side show response of the $D\alpha$ filterscopes for the two shots individually.

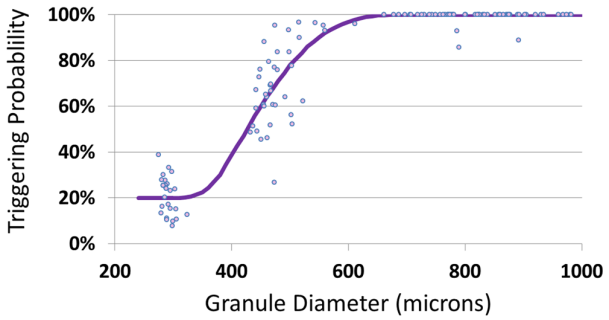

Figure 8. Triggering efficiency dependence on granule diameter. Each dot represents the average size and triggering efficiency for a 100 ms block of granules. The smooth fit line, used to guide the eye, shows a threshold below which the injection of a granule will not necessarily result in the prompt triggering of an ELM. Probabilities determined for the smallest size granules are believed to be representative of coincidental timing between granule injection and ELM triggering.

coincidentally but not causally with a granule is also approximately 20%, thus leading to the inference that there is no correlation between a specific granule and the triggering of a specific ELM for small granule sizes. This is likely due to the smaller granules generating insufficient perturbations atop the H-mode pressure pedestal, i.e. too small for ELM triggering. Collectively, however, the injection of these sub-threshold granules can result in a substantial increase in the effective ELM frequency, as discussed in section 4.4.

4.2. Super-threshold granule injection

Above a diameter of 600 microns, corresponding to 5.5×10^{18} Li atoms, injected granules are capable of individually triggering an ELM greater than 95% of the time. The granule-triggered ELMs are then combined with the spontaneously occurring ELMs, boosting the frequency. During EAST 70601, granule injection was able to boost the ELM frequency by 36%, from 275 Hz to 375 Hz, thus indicating that the 80 Hz granule injection was successful in supplementing the natural ELM frequency. This behavior can be seen in panels (*a*) and (*c*) of figure 9 which display the $D\alpha$ and XUV diode traces, as well as the ELM frequency respectively. Panel (*b*) is a magnification of the traces from panel (*a*) showing the time from 5–5.9 s. The right hand side of this panel shows that each granule injection, as represented by a peak on the blue XUV trace, corresponds to a similar peak in the $D\alpha$ trace.

As can be seen in the left hand side of panel (*b*), oscillations have been observed on EAST during situations of high I_p and heating power similar to the discharges seen here. To determine the type of instability inherent in the discharge we examine the upper and lower $D\alpha$ traces. If the instability manifests as a vertical wobble, the oscillations in the signal will be out of phase. If the instability is represented by an in–out mode, the oscillations should align. The synchronized behavior of the oscillations prior to granule injection shows that the large peaks seen in the $D\alpha$ trace can be interpreted as an in–out fluctuation of the overall discharge. As can be seen, the injection of these large granules has the effect of removing the oscillation from the unperturbed discharge. We postulate that the introduction of the granules reduces the edge current density thus leading to an increase in stability. Precision edge profile measurements to test this postulate were unavailable for these discharges.

The observation of a granule pacing factor near unity for this discharge as well as EAST 70602 indicates that these granules are not only successful in triggering ELMs, but that these ELMs occur in addition to the previously initiated natural ELMs. This is in contrast to EAST 70603 and 70604 where the per granule triggering efficiency is still near 100%, however the slight decrease in size and increased rate of granule injection leads to a situation whereby the injected granules are starting to generate ELMs which replace the naturally occurring ELMs. Thus the ELM triggering frequency is only raised by approximately 60 Hz, leading to a pacing

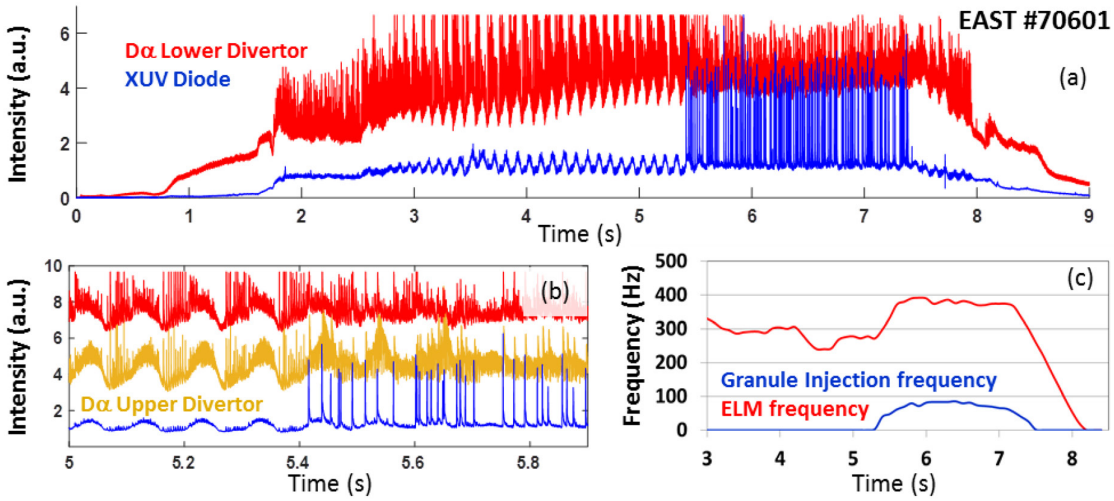

Figure 9. PXUV and $D\alpha$ traces from EAST discharge #70601. Panel (*a*) shows 900 micron granules injected from approx. 5.5–7.5 s. Panel (*b*) displays simultaneous oscillations on Da upper and lower divertor diagnostics which are suppressed by granule injection. Panel (*c*) shows that the injection of granules at approximately 80 Hz increases the ELM frequency by a commensurate amount.

factor closer to 50%. Recall that to achieve a mitigation effect from an elevated ELM frequency we are only looking for an increase in the global ELM triggering rate without a particular dependence on the nascent cause of the ELM.

4.3. Threshold granule injection and intra-shot granule size variation

For lower granule sizes, the ability of a particular injected granule to trigger an ELM becomes less certain. We postulate that these granules are of borderline size, i.e. the granule will trigger an ELM if and only if the pedestal conditions within the discharge are already close to instability. This postulate conceptually would account for a portion of the wide range in triggering efficiencies seen with these smaller granules. Examining EAST 70606 as shown in figures 6 and 7, we can see that the injection of 460 micron granules at a drop frequency of 1239 Hz led to an increase in the ELM triggering frequency by a factor of 2.2×, and a reduction in the peak $D\alpha$ intensity by a factor of 1.7×.

4.3.1. Intra-shot granule size variation. In the upper reservoir of the dropper assembly there are four independent chambers which house alternate granule sizes [17, 19]. When a chamber is selected the granules in that chamber fall onto the top of a piezoelectric disk which, when activated, drives them towards the drop tube. When changing the granule injector from one size granule to another, nominally the first chamber is closed and the piezo is then activated to clear the remaining old granules from the disk face prior to the transition to an alternate granule size. If however the disk is not activated for a sufficiently long period, the granules can remain. Upon accessing a new chamber there can thus exist a temporary superposition of the two granule sizes, with the old size closer to the opening and the newer size displaced radially outward from the hole. At the next activation of the disk, the ejected granules will be replaced with the newer granules, until the transition is complete. EAST discharge 70605 contained just such a transition from large to small granules.

It is a characteristic of the operation of the granule dropper that, as the diameter of the granule decreases, the frequency of the granule drop increases for a similar piezo excitation voltage. Thus as we dynamically decreased the average granule size throughout the discharge as shown in figure 10, we observed an increase in the number of granules injected within the examination window. Statistically, monitoring the average granule size over the course of discrete 100 ms blocks during the discharge showed that the initial granule diameter was approximately 800 microns, consistent with the average granule size from the two previous discharges. This continued for the next second of granule injection, then over the course of the next two seconds of granule injection, the average granule size dropped quickly to 600 microns in diameter, and then more gradually to just under 500 microns.

This drop in granule size resulted in a commensurate drop in the averaged triggering efficiency for the same period of time. However the increase in granule injection frequency outpaced the decrease in ELM triggering efficiency leading to an overall increase in effective ELM triggering frequency. In addition to the observed increase in the average ELM frequency we also note a reduction in the peak $D\alpha$ signals which we interpret as a reduction in the ELM size. At the end of the discharge the overall triggering efficiency dropped to 60%, consistent with the values seen throughout the next discharge (EAST #70606) of 65% with 460 micron granules.

4.4. Sub-threshold granule injection

As the granule drop rate increases it is possible for multiple granules to drop into the injection chamber between impeller passes, and thus be injected at the same or similar times. While multiple injections did not occur often for the largest granules, it was routine for the smaller granules used in this work. For these small granules, the granule drop frequency

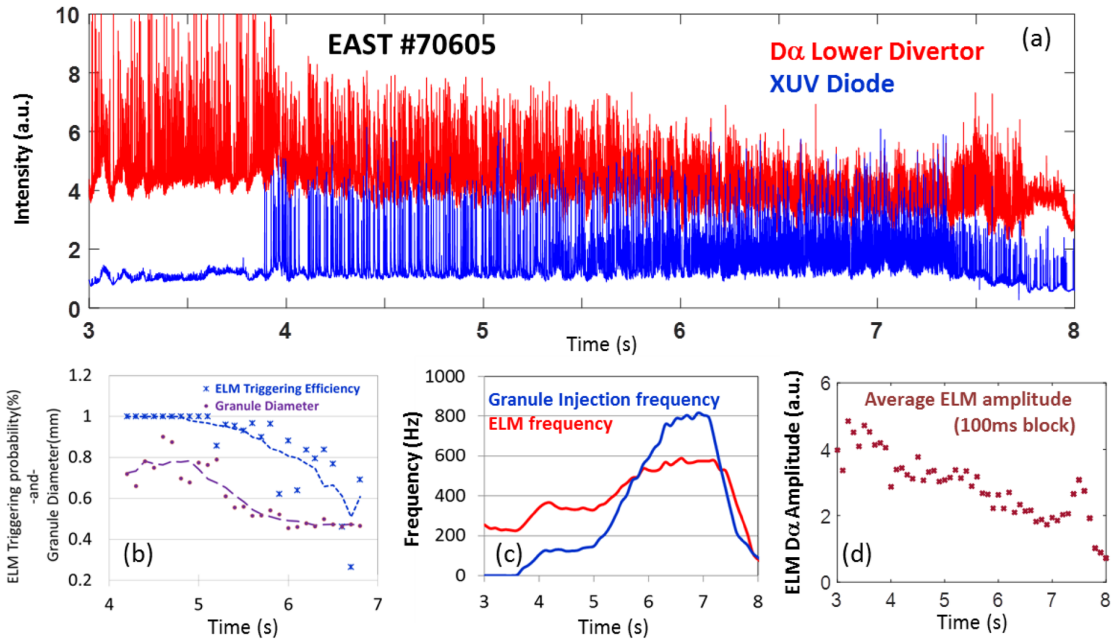

Figure 10. Variable size and frequency granule injection from EAST discharge #70605. As described in the text, over the course of the discharge, the size of the injected granules, shown in panel (*b*) decreases from 800 microns to just above 400 microns. In addition the granule injection frequency increases from 100 Hz to 800 Hz leading to an increase in ELM frequency from 200 Hz to 600 Hz as shown in panel (*c*). This increase in ELM frequency leads to a decrease in the overall ELM amplitude (peak height above baseline) by a factor of greater than 2 as is shown in panel (*d*).

could exceed the impeller frequency by roughly a factor of 10 × at even a moderate piezo voltage. This resulted in an overlapping cascade of granules and multiple injection events per impeller pass. As can be seen in figure 11, each pass of a single impeller blade was responsible for the delivery of over a dozen small granules. As such it was impractical to track individual granules as was done with the larger sizes. However we can state that the cluster of granules was able to penetrate the edge of the discharge at multiple points and with multiple entry angles, thus creating a 'condition' at the plasma edge, as opposed to a single track of injected mass as with the larger granules. An additional effect of this multiple granule injection is that variations in strike angle with the impeller face and granule impeller coupling resulted in a spread in the transit times from the impeller to the plasma edge. This spread had the effect of temporally smearing-out the injection of a cluster of granules. The consequence of these effects is an overall granule injection frequency as measured by the XUV diagnostic that can be up to 4 × larger than the impeller frequency, with the actual frequency of granule injection being higher still.

As the granule size is reduced, the impediment to free flow for the granules is also diminished, i.e. controllability of the injection rate is lost. This had an effect on the controlled operation of the dropper section of the granule injector. Once the selection door was rotated to the chamber containing the smallest granules, these granules began to free flow out of the reservoir and down the drop tube independent of agitation of the piezoelectric disk. Thus in order to control the delivery of the granules, the quadrant door needed to be quickly opened and closed, thus depositing a quantity of granules onto the disk without the pressure of the remaining inventory driving them toward the drop tube. This deposited a small quantity of granules onto the piezo face sufficient for a single multi-second discharge. A consequence of this loading procedure is a declining granule injection rate during the course of the discharge. As is visible in figure 12, the granule injection rate started at approximately 20 granules per impeller pass at the beginning of the injection period and dropped to less than 5 granules per impeller pass as the injection concluded. This corresponded to an observed injection rate from XUV data of 1200 Hz at the beginning of the injection period which then declined to 600 Hz during the course of the discharge.

Passing below the granule size triggering threshold, the injected granules show no concrete correlation with the triggering of an ELM. Previous experiments and non-linear MHD modelling with the JOREK code [31] show that the ability of an injected granule or pellet to trigger an ELM corresponds directly with the ability of that injected mass to reach the top of the H-mode pedestal and contribute to the pre-existing pressure gradient. Thus granules which fully ablate prior to that point are unable to trigger an ELM, an observation borne out with the injection of the smallest size granules. Despite the low occurrence of individual ELM triggering, there is, nonetheless, a direct beneficial effect of multiple sub-threshold granule injection on ELM behavior. As evident in the $D\alpha$ traces, the injection of granules leads to an increase in the ELM frequency from 250 Hz to nearly 700 Hz. This is also reflected in a reduction of the height of the $D\alpha$ peak amplitude above the baseline $D\alpha$ signal. Examining the $D\alpha$ traces

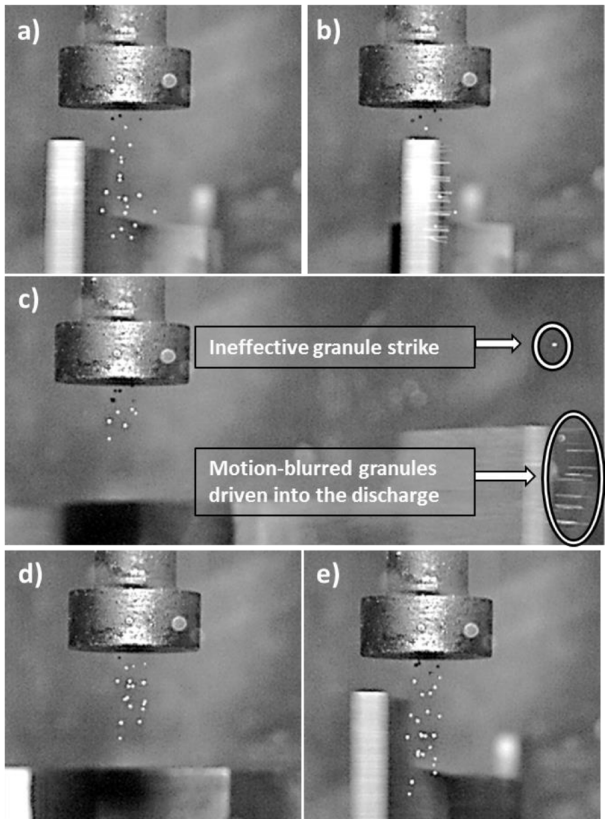

Figure 11. Simultaneous multiple-granule injection. These frames show the injection cycle for multiple small (<300 micron) granules. Time delay between frames (*a*) and (*b*) is 100 μs. Delay from (*b*) and (*c*) is 800 μs, and from (*a*)–(*e*) is 3.8 ms. Frame (*c*) shows the majority of the granules being injected.

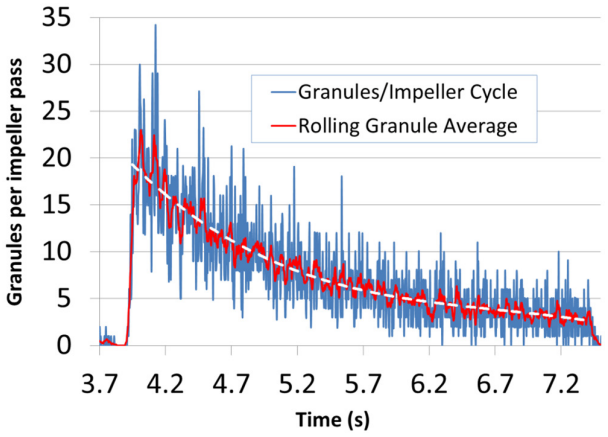

Figure 12. Granules injected per impeller pass. The underlying blue trace is a record of the number of granules injected during each pass of the impeller. To better characterize the general trend a rolling average of 5 impeller passes is also displayed in red, with a polynomial fit to the decay displayed as the dotted line. The overall behavior is indicative of a small volume of granules being depleted during the discharge.

in figure 13, it can be seen that the size and duration of the ELMs was reduced by greater than a factor of 2. Also there is a mild recovery of the ELM intensity during the decay in

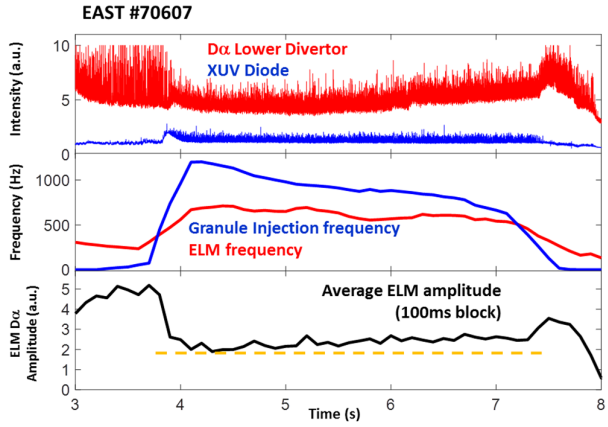

Figure 13. EAST 70607 sub threshold mitigation of ELM intensity: granules of approximate diameter of 260 microns, with multiple granules injected per pass, reduce peak ELM intensity by a factor of 2. Note that the reduction in granule injection frequency over the course of the discharge is the result of fewer granules being injected per impeller pass, and thus a reduction in the injected mass, not the actual granule injection frequency. This reduction in edge perturbation leads to a mild recovery of the average ELM amplitude as shown by the slope of the lowest graph from 4–7 s. The horizontal dotted line is inserted to guide the eye.

injection frequency, as evidenced by the decline on the blue trace in the middle panel of figure 13.

Thus we have mitigated the effects of ELMs through a modification of the discharge edge as a result of multiple sub-threshold granule injection. These results stand in comparison to the more familiar 'one-granule-one-ELM' scenario for ELM mitigation.

5. Summary and conclusions

We have demonstrated that injection of impurity granules can both trigger individual ELMs and also generate an overall increase in ELM frequency, even when the granules are below the individual size threshold needed for ELM destabilization. The prompt triggering of an ELM in EAST is primarily dependent upon the size of the injected granule. Granules above 600 μm in diameter trigger ELMs nearly 100% of the time. However the ability of the granules to augment the ELM frequency by an amount corresponding to the triggering frequency was only found to be applicable for injection frequencies below 100 Hz. Triggering rates greater than 100 Hz led to the replacement of spontaneous ELMs with stimulated ELMs.

For granules smaller than the empirically determined triggering size threshold, the efficacy of a single granule in promptly triggering an ELM generally decreased with granule size to ~20%, corresponding to the statistical probability of a coincidental timing between granule injection and temporal proximity to a naturally occurring ELM. Hence for these small granules it is unlikely that the triggering of an ELM was the result of any single granule.

Nonetheless an overall increase in the ELM frequency with increasing small granule injection frequency was observed, along with a decrease in ELM amplitude. Thus sub-threshold

granule injection to augment the natural ELM frequency has been demonstrated, as opposed to the 1:1 granule-to-ELM triggering in previous studies. This augmentation could prove to be a more robust method for ELM control in future devices, provided that the core and edge discharge parameters can be maintained at design values. While ITER has programmatically decided against use of lithium within the vacuum vessel due to the tritium retention properties of the material, there is no reason to believe that the ELM triggering resultant from granule induced pressure perturbations could not be replicated by ITER relevant low Z materials such as beryllium and boron. To that end granule induced ELM triggering with alternate materials is recommended as a future step for this research.

Acknowledgments

This research is funded by National Key Research and Development Program of China (2017YFE0301100 and 2017YFA0402500), National Nature Science Foundation of China (11775261, 11625524, 11605246, 11075185 and 11021565) and in part by the U.S. Department of Energy under contract DE-AC02-09CH11466, DE-FG02-09ER55012 and DE-FC02-04ER54698. We gratefully acknowledge the contributions from the EAST technical staff. The digital data for this paper can be found at http://arks.princeton.edu/ark:/88435/dsp01zc77ss87k.

ORCID iDs

R. Lunsford https://orcid.org/0000-0003-3588-6801
Z. Sun https://orcid.org/0000-0002-7224-3592

References

[1] Loarte A. *et al* 2003 *Plasma Phys. Control. Fusion* **45** 1549
[2] Eich T. *et al* 2013 *Nucl. Fusion* **53** 093031
[3] Zhitlukhin A. *et al* 2007 *J. Nucl. Mater.* **363–5** 301–7
[4] Zohm H. *et al* 1996 *Plasma Phys. Control. Fusion* **38** 105
[5] Loarte A. *et al* 2007 Progress in the ITER physics basis chapter 4: power and particle control 2007 *Nucl Fusion* **47** S203
[6] Baylor L.R. *et al* 2013 *Phys. Rev.Lett.* **110** 245001
[7] Evans T.E. 2013 *J. Nucl. Mater.* **438** S11–8
[8] Guo H.Y. *et al* 2014 *Nucl. Fusion* **54** 013002
[9] Song Y.T. *et al* 2014 *IEEE Trans. Plasma Sci.* **42** 503–9
[10] Wan B.N. *et al* 2015 *Nucl. Fusion* **55** 104015
[11] Zuo G.Z. *et al* 2012 *Plasma Phys. Control. Fusion* **54** 015014
[12] Hu J.S. *et al* 2015 *Phys. Rev. Lett.* **114** 055001
[13] Hu J.S. *et al* 2015 *J. Nucl. Mater.* **463** 718–22
[14] Sun Y. *et al* 2017 *Nucl. Fusion* **57** 036007
[15] Yuan X.L. *et al* 2018 *Fusion Eng. Des.* **126** 130–8
[16] Wang L. *et al* 2013 *Nucl. Fusion* **53** 073028
[17] Mansfield D.K. *et al* 2013 *Nucl. Fusion* **53** 113023
[18] Mansfield D.K. *et al* 2010 *Fusion Eng. Des.* **85** 890
[19] Sun Z. *et al* 2018 *IEEE Trans. Plasma Sci.* **46** 1076
[20] Roquemore A.L. *et al* 2011 *Fusion Eng. Des.* **86** 1355
[21] Kuninaka H. and Hayakawa H. 2004 *Phys. Rev. Lett.* **93** 154301
[22] Lunsford R. *et al* 2018 *Nucl. Fusion* **58** 036007
[23] Bortolon A. *et al* 2016 *Nucl. Fusion* **56** 056008
[24] Müller H.W. *et al* 2002 *Nucl. Fusion* **42** 301
[25] Kocsis G. *et al* 1999 *Plasma Phys. Control. Fusion* **41** 881–98
[26] Pégourié B. 2007 *Plasma Phys. Control. Fusion* **49** R87–R160
[27] Parks P.B. *et al* 1988 *Nucl. Fusion* **28** 477
[28] Parks P.B. *et al* 1994 *Nucl. Fusion* **34** 417
[29] Rozhansky V.A. and Senichenkov I.Yu. 2005 *Plasma Phys. Rep.* **31** 993
[30] Huysmans G.T. *et al* 2009 *Plasma Phys. Control. Fusion* **51** 124012
[31] Futatani S. *et al* 2014 *Nucl. Fusion* **54** 073008
[32] Bortolon A. *et al* 2017 *Nucl. Mater. Energy* **12** 1030–6
[33] Lang P.T. *et al* 2004 *Nucl. Fusion* **44** 665–7
[34] Lang P.T. *et al* 2013 *Nucl Fusion* **53** 073010
[35] Lang P.T. *et al* 2014 *Nucl Fusion* **54** 083009
[36] Maingi R. *et al* 2012 *Nucl Fusion* **52** 083001
[37] Maingi R. *et al* 2018 *Nucl. Fusion* **58** 024003
[38] Canik J.M. 2018 *IEEE Trans. Plasma Sci.* **46** 1081
[39] Baylor L.R. 1999 *J. Nucl. Mater.* **266–9** 457